Korean J. Chem. Eng., 36(7), 1082-1089 (2019)
DOI: 10.1007/s11814-019-0274-2

pISSN: 0256-1115
eISSN: 1975-7220

Mechanisms of dry flue-gas desulfurization using natural manganese oxide ores

Yongxiang Chen*, Yunjiao LI*,†, Xinlong Cao*,*, Jianguo Li*, Sanchuan Tang**, Wanqi Ye*, and Xianzhen Zhang***

*School of Metallurgy and Environment, Central South University, Changsha 410083, P. R. China
**Changsha Research Institutes of Mining and Metallurgy, 966 Lushan South Road, Changsha 410012, P. R. China
***Shaanxi Coal Chemical Industry Technology Research Institute Co. Ltd. Xian 710075, P. R. China
(*Received 6 January 2019 • accepted 9 April 2019*)

Abstract−The mechanisms of flue-gas desulfurization using high and low-grade natural manganese oxide ores were comparatively studied. Both manganese oxide ores exhibit good desulfurization capabilities with SO_2 content in the effluents less than 30 ppm, but the low-grade ores show the much better desulfurization capability. XRD and SEM/EDS results reveal that the MnO_2 absorbs the SO_2 to convert to $MnSO_4$. The SO_2 give prior to react with the surface MnO_2 and the produced $MnSO_2$ enriched on the surface leads to the gradually decrease of the SO_2 removal rate during desulfurization process. The better desulfurization capability of the low-grade ores is ascribed to the more dispersive MnO_2 due to the poriferous/lax internal tunnel structure, and the embedded inert SiO_2 shows better support effects to avoid pore structure blocking, which is favorable for enhancing the diffusion of the SO_2 and desulfurization reaction process. This study is of significance in the comprehensive utilization of the low-grade natural manganese oxide ores, environmental protection and even the preparation of the desulfurization catalyst with MnO_2.

Keywords: Mechanism, Manganese Oxides, Manganese Sulfate, Flue-gas Desulfurization

INTRODUCTION

Sulfur oxides (SO_x) are the major hazardous air pollutants in flue gas, which contributes to regional acid rain pollution and urban photochemical smog [1-3]. Therefore, sulfur oxides (SO_x) must be cleaned before being emitted. In particular, sulfur dioxide (SO_2) generated from coal and fossil oil combustion is one of the major anthropogenic contributors to air pollution [1]. Typically, China is one of the few countries in the world where more than 70% of the country's total energy sources are supplied by coal combustion. Thus, flue-gas desulfurization (FGD) appears particularly important. At present, the most successful and commercialized desulfurization technology is wet flue gas desulfurization (WFGD), especially wet limestone FGD [4,5]. Although this technology can meet the regulatory requirements for the control of sulfur dioxide emissions and the raw materials are easily obtained, some issues cannot be ignored. First, the byproducts of this process can easily plug pipes and be normally discarded as voluminous liquid slurry, which can lead to secondary contamination [6]. Secondly, the temperature of flue gas flowing towards the reactor tower usually needs to be cooled to 85-100 °C from 300 °C, which makes the waste heat of flue-gas not effectively utilized. After aqueous phase absorption, the temperature of flue gas may drop to 40-50 °C, which is unfavorable for gas emissions. In recent years, some other WFGD technologies, such as double alkalis FGD and seawater FGD, have been further studied to improve on these drawbacks [7-9]. These technologies have advantages in some aspects and are used in some factories, but some deficiencies are still unavoidable, such as pipe blockage, secondary contamination, high operating costs, which lead some technologies to be difficult to promote in the actual industrial process [7,10-15].

Dry FGD technologies are considered to solve those issues because the flue gases can directly contact with dry sorbents (lime, activated carbon et al.). Compared with the wet FGD, the dry FGD is considered to be the more suitable way of flue gas desulfurization because of the low operating costs, no water consumption and easy treatments of the byproducts [16-18].

Recently, a significant amount of work has been done to develop dry FGD processes based on the sorption of sulfur oxides on metal oxide [19-21]. In those dry sorbents, manganese oxides (MnO_x) have been investigated due to the high sulfur dioxide absorption capacity, which is based on MnO_6 octahedral sharing faces and edges to form various tunnel structures [22,23]. A few researchers focus on dry flue-gas desulfurization using manganese oxides (ores) as sorbents from the 1960s, and the effects of various parameters, such as temperature, SO_2 concentration, O_2 concentration and space velocity are studied in detail. These studies indicate that manganese oxides (ores) have high SO_2 absorption capacity and the manganese sulfate byproduct is easy to use without secondary pollution [24-26]. However, most of the studies use synthetic rather than natural manganese oxides absorbent. The preparation of the absorbents increases the cost of desulfurization to some extent. In addition, many of them only pay attention to the desulfurization performance of the absorbents, while the mechanisms of the desulfurization rate decreasing at the late stage of the reaction have been ignored. Therefore, it is meaningful to find manganese oxides cheaper absorbent

†To whom correspondence should be addressed.
E-mail: yunjiao_li@csu.edu.cn

Table 1. The chemical composition of the manganese oxide ores (wt%)

Ore type	Mn	Fe	Si	Al	Na	Ca	K	Mg	S
High-grade	58.75	0.91	1.71	1.04	0.945	0.37	0.75	0.026	0.061
Low-grade	20.81	8.91	16.19	5.52	0.46	0.64	1.67	0.74	0.025

to achieve high-efficient flue gas desulfurization. Lu Fan et al. studied the activated carbon supported pyrolusite on desulfurization [20] and found that the higher sulfur capacity of pyrolusite activated carbon is mainly attributed to the synergistic effect of metals mixture (manganese and iron) in pyrolusite. The natural manganese oxide ores have been confirmed to be better for desulfurization. However, the desulfurization capabilities of the different grade natural manganese ores have not been reported comparably and the desulfurization mechanisms of the different grade natural manganese ores are also not investigated.

In this study, two natural manganese oxide ores with different grades were selected as the raw materials to study flue gas desulfurization comparatively. The behaviors of high and low-grade manganese ores on desulfurization were studied, which reveal the mechanisms of the dry flue-gas desulfurization with natural manganese oxide ores. The results provide a theoretical basis for strengthening the desulfurization process. In addition, it is believed that this study is of significance in co-utilizing of the low-grade natural manganese oxides ores and SO_2 in flue gas, environmental protection and even the preparation of the desulfurization catalyst with MnO_2.

EXPERIMENTAL

The low and high-grade natural manganese oxide ores used in this study were provided by Citic Dameng Co., Ltd. Guangxi Zhuang Autonomous Region, China. The two types of natural manganese oxide ores were crushed, ground, and then sieved to 80-120 μm. The components were analyzed by atomic absorption spectrophotometer (TAS-990, PGENERAL, China).

Manganese oxide ores (15 g) were fed into the fluidized bed reactor and heated to 723 K. Then the simulated flue gas mixture containing 2,000 ppm SO_2, 5% O_2 and balance N_2 was introduced in the quartz tube reactor at a gas space velocity of 3,200 mL/g·h^{-1} (GHSV) and reacted with the ores for a certain time. The reaction time was 8 h. During the reaction, the effluent SO_2 concentration was measured on-line by portable gas analyzer PG-350 (HORIBA, Japan). At the end of the processes, the reactor was cooled and solid samples were taken out for analysis. The SO_2 removal rate was calculated by equation as follows:

$$R_1=(C_1-C_2)/C_1\times100\% \quad (1)$$

where R_1 is SO_2 removal rate, C_1 and C_2 are the concentrations of SO_2, in ppm, at the inlet and outlet of the reactor, respectively. The breakthrough capacity is defined as the point where the SO_2 out exceeded 30 ppm.

X-ray powder diffraction (TTR III, Rigaku Corporation, Japan) with Cu Kα radiation at a speed of 10°·min^{-1} was employed to characterize the structures of the ores and the desulfurization products. The specific surfaces were measured by the surface area and porosity analyzer (ASAP2020 HD88, America). The adsorption data was then used to calculate the surface area using the Brunauer-Emmett-Teller (BET) equation. The section of the particles was observed through a JSM-6360LV scanning electron microscope (SEM, JEOL, Japan) with an applied voltage of 20 kV. Scanning electron microscopy equipped with an energy dispersive X-ray spectrometer was used for the elemental analysis of the morphology and sectioned specimens.

RESULTS AND DISCUSSION

1. Components and Phase Structure of the Manganese Oxide Ores

Atomic absorption spectrophotometry (AAS, TAS-990, PGENERAL, China) was carried out to obtain the components of the both manganese oxide ores. The chemical compositions obtained AAS are listed in Table 1. Both manganese oxide ores show different manganese content. For the high-grade manganese oxide ores, the Mn content (wt%) is 58.75 wt%. The low-grade manganese oxide ores contain 20.81 wt% Mn, 8.91 wt% Fe, 16.19 wt% Si and 5.52 wt% Al.

Fig. 1 depicts the X-ray powder diffraction (XRD) patterns of the both manganese oxide ores. Both samples show remarkable MnO_2 peaks, but some peaks appearing in the two samples are different. Typically, high-grade manganese oxide ores mainly include α-MnO_2 (marked with **1**) and minor Mn_2O_3 (marked with **4**), and the MnO_2 with other structures are negligible due to the low content. And for the low-grade manganese oxides ores, one can observe that there are significantly great sharper and stronger diffraction peaks (marked as **5**), indexed with the SiO_2 phase, demonstrating

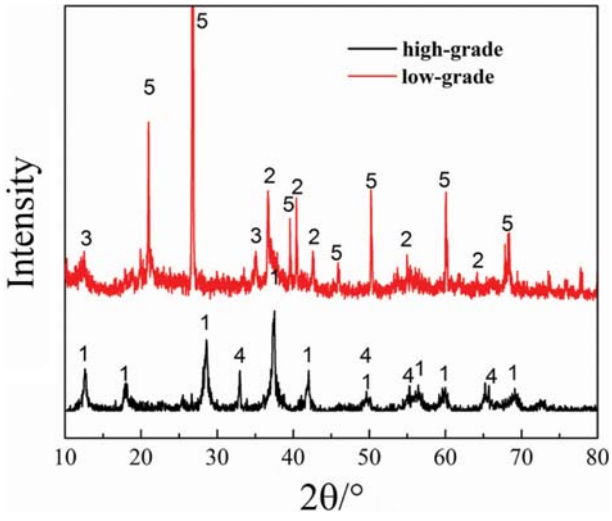

Fig. 1. XRD patterns of the fresh manganese oxide ores (1: α-MnO_2; 2: γ-MnO_2; 3: δ-MnO_2; 4: Mn_2O_3; 5: SiO_2).

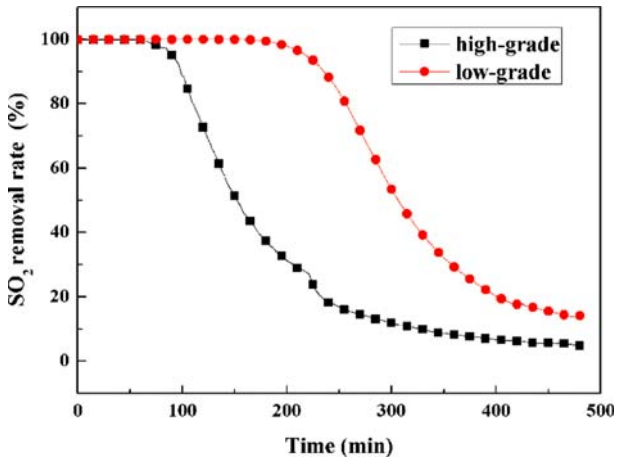

Fig. 2. The relationship between SO_2 removal rate and retention time of the low and high-grade manganese oxide ores.

the good crystallinity and relatively large content of SiO_2. Unlike the high-grade manganese oxide ores, there still exist some small peaks of γ-MnO_2 and δ-MnO_2 marked in **2** and **3**, respectively, except for the α-MnO_2. No other phases like Fe_2O_3 and Al_2O_3 compounds are detected due to their low content or crystallinity.

2. Flue Gas Desulfurization Curve

Fig. 2 shows the SO_2 removal rate *vs.* retention time curves of different-grade manganese oxide ores in the flue gas desulfurization process. Both samples show similar desulfurization process, but the flue-gas desulfurization abilities are quite different. In particular, the SO_2 removal rate of the high-grade manganese oxides is more than ~99% with SO_2 less than 30 ppm in the initial 90 min and then rapidly drops to ~35% at 200 min, and then gradually decreases to only 5.3% at 480 min. As for the low-grade manganese oxides, the retention time of the SO_2 removal rate around 99% maintains about 200 min, and it reaches to ~14.3% even at 480 min. Both of the manganese oxides ores exhibit good flue-gas desulfurization ability at the beginning to some extent. However, the SO_2 removal rates gradually decline to a relatively stable level, indicating the flue-gas desulfurization ability fading for both samples. Obviously, the longer retention time with ~99% SO_2 removal rate for the low-grade manganese oxides indicates the much better flue-gas desulfurization ability, which is very meaningful for the effective use of natural manganese oxide ore resources, especially for low-grade manganese oxide ores.

3. Phase Structural Change After Desulfurization

XRD was performed to investigate the phase composition of the two manganese oxides ores after desulfurization. As shown in Fig. 3, some new peaks around 2θ=24°, 25.4° and 33.1°, respectively, indexed with $MnSO_4$ phase, clearly appear in both sulfated manganese oxide ores. And part of the MnO_2 peaks become weak or disappear, indicating the MnO_2 partially converts into $MnSO_4$ in the desulfurization process. While, the peaks of Mn_2O_3 phase in high-grade manganese oxide ores are still detected after desulfurization. It is difficult to judge whether the Mn_2O_3 phase participates in the desulfurization reaction in the case. Thus, the pure Mn_2O_3 suffered from the same desulfurization process and then the sulfated product was detected by XRD. As shown in Fig. S1,

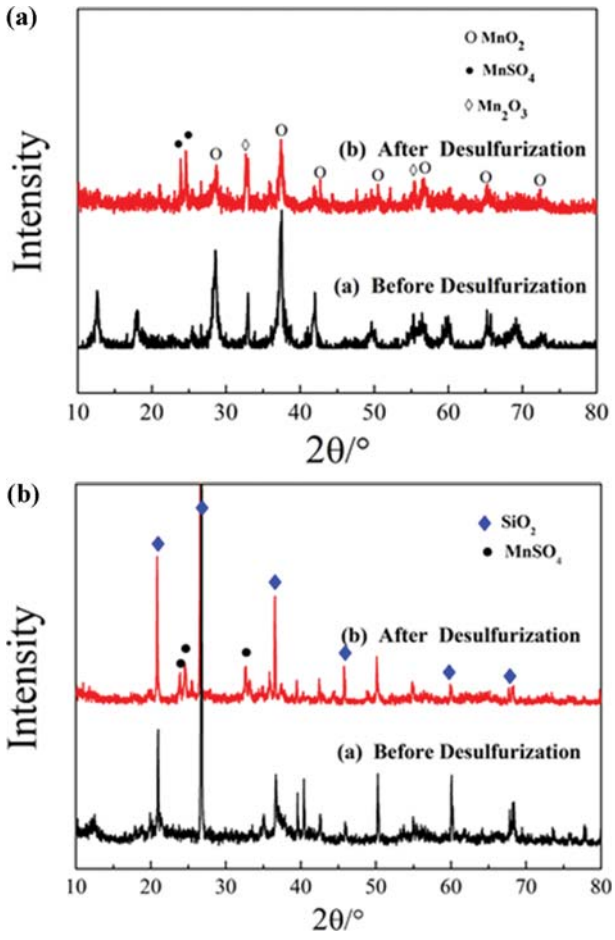

Fig. 3. XRD patterns of the fresh and sulfated manganese oxides ores ((a) High-grade ores; (b) low-grade ores).

some typical $MnSO_4$ peaks can be found in the sulfated product, demonstrating the Mn_2O_3 can also react with the SO_2 in the desulfurization process. The Fe content in the low-grade manganese oxides ores reached 8.91 wt%. According to previous studies [17, 27], Fe_2O_3 is the main phase in the manganese oxides ores and shows some sulfur capacity under certain conditions. Therefore, it is necessary to further investigate the desulfurization ability of Fe_2O_3 in the process. As shown in Fig. S2, there is no variation in the peaks of the Fe_2O_3 phase before and after desulfurization for the pure Fe_2O_3, indicating that the removal of SO_2 is not affected by the Fe_2O_3. As a result, it can be concluded that the SO_2 in flue gas is mainly adsorbed by the manganese oxide ores to produce $MnSO_4$. The chemical reactions are listed as follows:

$$MnO_2+SO_2=MnSO_4$$

$$2Mn_2O_3+4SO_2+O_2=4MnSO_4$$

4. Manganese Conversion Rate

Based on reaction (1) and (2), the Mn conversion rates from the manganese oxides to $MnSO_4$ during desulfurization are directly associated with the SO_2 removal rate. The high Mn conversion rates represent high Mn utilization efficiencies. Thus, it is necessary to measure the manganese conversion rates to evaluate the manga-

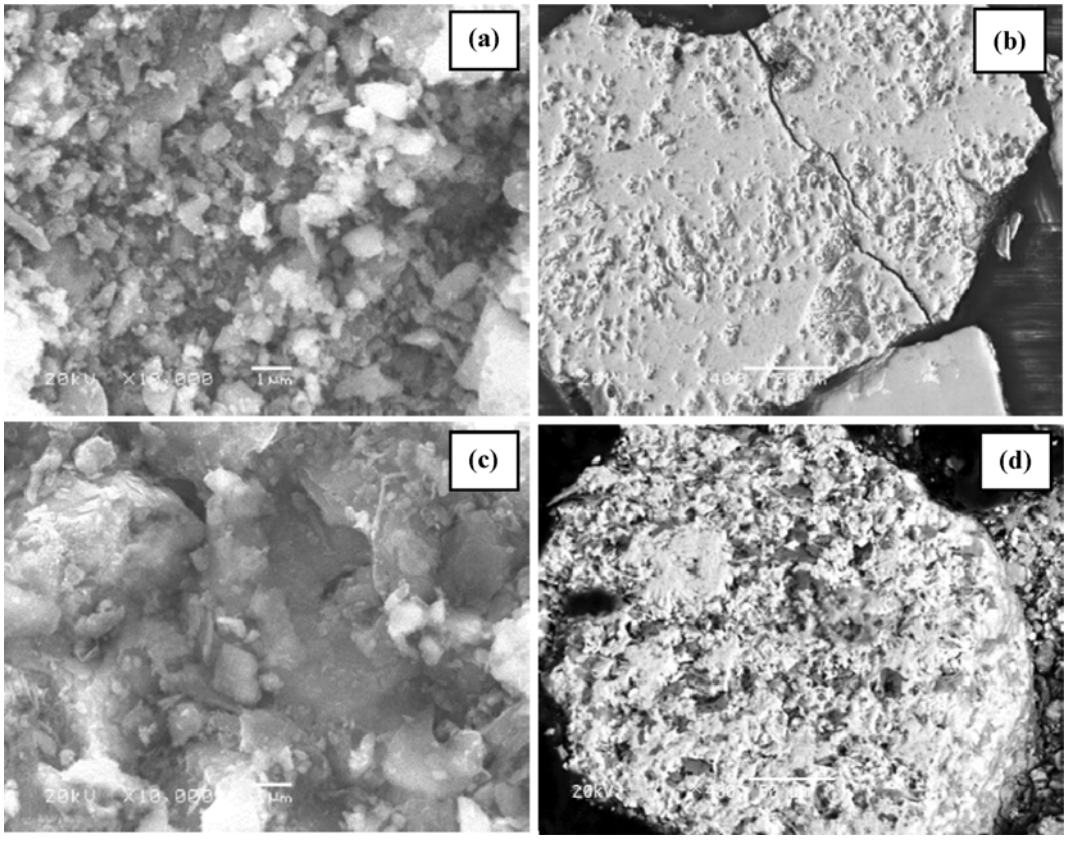

Fig. 4. SEM and the cross-section images of the different grade manganese oxides: (a), (b) High-grade manganese oxides ores; (c), (d) low-grade manganese oxides ores.

nese utilization efficiencies. The detailed methods are shown as follows:

The obtained sulfated manganese oxide ores samples taken, one was stirred in deionized water to dissolve the soluble manganese salts (mainly $MnSO_4$). And the other one with the same weight was leached in aqua regia to dissolve the total Mn. Mn content in obtained solutions was measured by AAS. The manganese conversion rates are calculated as follows:

$$R_2=C_3/C_4\times100\% \quad (2)$$

where R_2 is manganese conversion rate, C_3 and C_4, in wt%, are the contents of the soluble Mn and total Mn, respectively. As a result, the manganese conversion rates at the end of the tests were 10.75% and 40.98% for the high and low-grade ores, respectively. Low Mn conversion rate of both ores implies the incomplete reaction during desulfurization and most of Mn in the sulfated manganese oxide ores still remains as oxide rather than $MnSO_4$, which agrees with the XRD analysis (Fig. 3). Comparatively, the low-grade one shows much higher manganese conversion rates than the higher one, which represents its higher manganese utilization efficiencies. This result is meaningful in the comprehensive utilization of the low-grade manganese oxide ores.

5. Morphological Characterization

The surface/internal morphology structures of the ores are in importance in the desulfurization reaction [20]. Scanning electron microscope (SEM) was applied to observe the morphologies of both samples. Fig. 4 shows the surface and the cross-section images of the two different manganese oxide ores before desulfurization. Both samples show rough surface structures. Notably, the high-grade manganese oxide ore (Fig. 4(a)) shows a loose surface with little granules distribution, while the low-grade manganese oxides ores in Fig. 4(c) is also loose and appears spongy-like structure. Moreover, the cross-sections of the particles were carried out (Figs. 4(b)-4(d)) to judge the internal structure. The high-grade manganese oxide ore (Fig. 4(a)) shows relatively dense and compact internal structure without obvious holes, while the low-grade manganese oxides ores are poriferous and lax structure with fine and small distributed holes. It is well known that a dense surface is unfavorable for gas adsorption and tends to hinder SO_2 diffusion toward the surface of the manganese oxides, which makes the SO_2 removal rate decrease [28]. The MnO_2 loaded on the poriferous and lax structure in low-grade manganese oxide ores may be favorable to SO_2 diffusion during desulfurization and further promotes flue-gas adsorption and manganese conversion. Both samples after desulfurization are observed by SEM/EDS in Fig. 5. The surface morphologies of both manganese oxides ores after desulfurization become flocculent and dense, which could be attributed to the manganese oxides converting to $MnSO_4$.

Fig. 6 exhibits the backscattered electron cross-section images of the sulfated high-grade manganese oxides corresponding to the EDS mapping. Typically, the Mn elements are distributed in the internal regions without very distinct differences except on the edge of

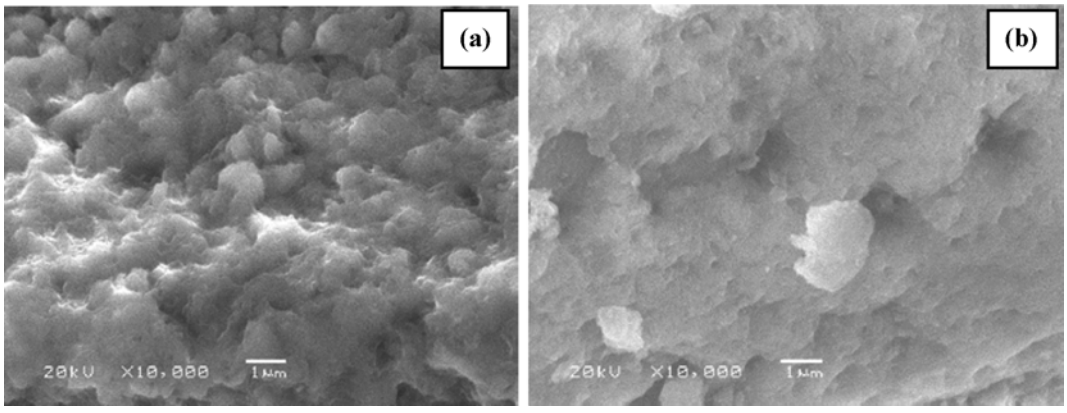

Fig. 5. SEM images of the different grade manganese oxides after desulfurization: (a) The high-grade manganese oxide ores and (b) the low-grade manganese ores.

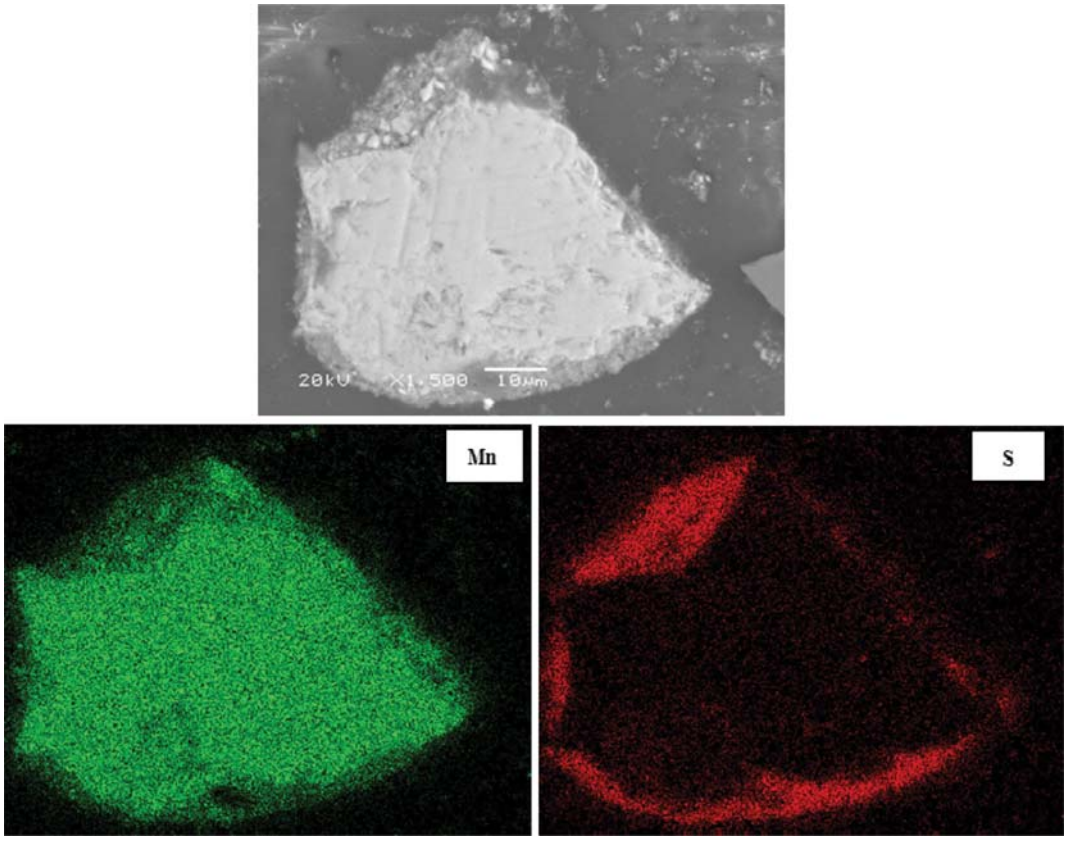

Fig. 6. Backscattered electron images of the sulfated high-grade manganese oxides section and surface scan results of the sulfated high-grade manganese oxides section.

the particles, which are relatively sparse, indicating the homogeneous distribution of Mn elements in the particle interior. S element is mainly distributed in the outer areas along with a tiny amount of S dispersed in the inner regions. This could be the SO_2 spreads to the interior through the loose surface structure of the manganese oxides ores at the beginning. The S distribution is consistent with the relatively sparse Mn distribution on the particle edges, demonstrating the produced $MnSO_4$ originated from S bonding with the Mn are mainly accumulated on the particle surface. With the increasing retention time, the surface $MnSO_4$ enrichment rapidly fills the surface pores and further hinders the diffusion of SO_2. Thus, the SO_2 removal rate shows a dramatic decline. With the reactions proceeding, the flocculent and dense surface structure are gradually strengthened by the produced $MnSO_4$, and then the SO_2 removal rate slightly declines [29]. When the retention time is enough long, the flocculent and dense surface hinder the SO_2 diffusion; thus the SO_2 removal rate then becomes stable at a low point.

An overall observation of the distributions of Si, Mn, Fe and S

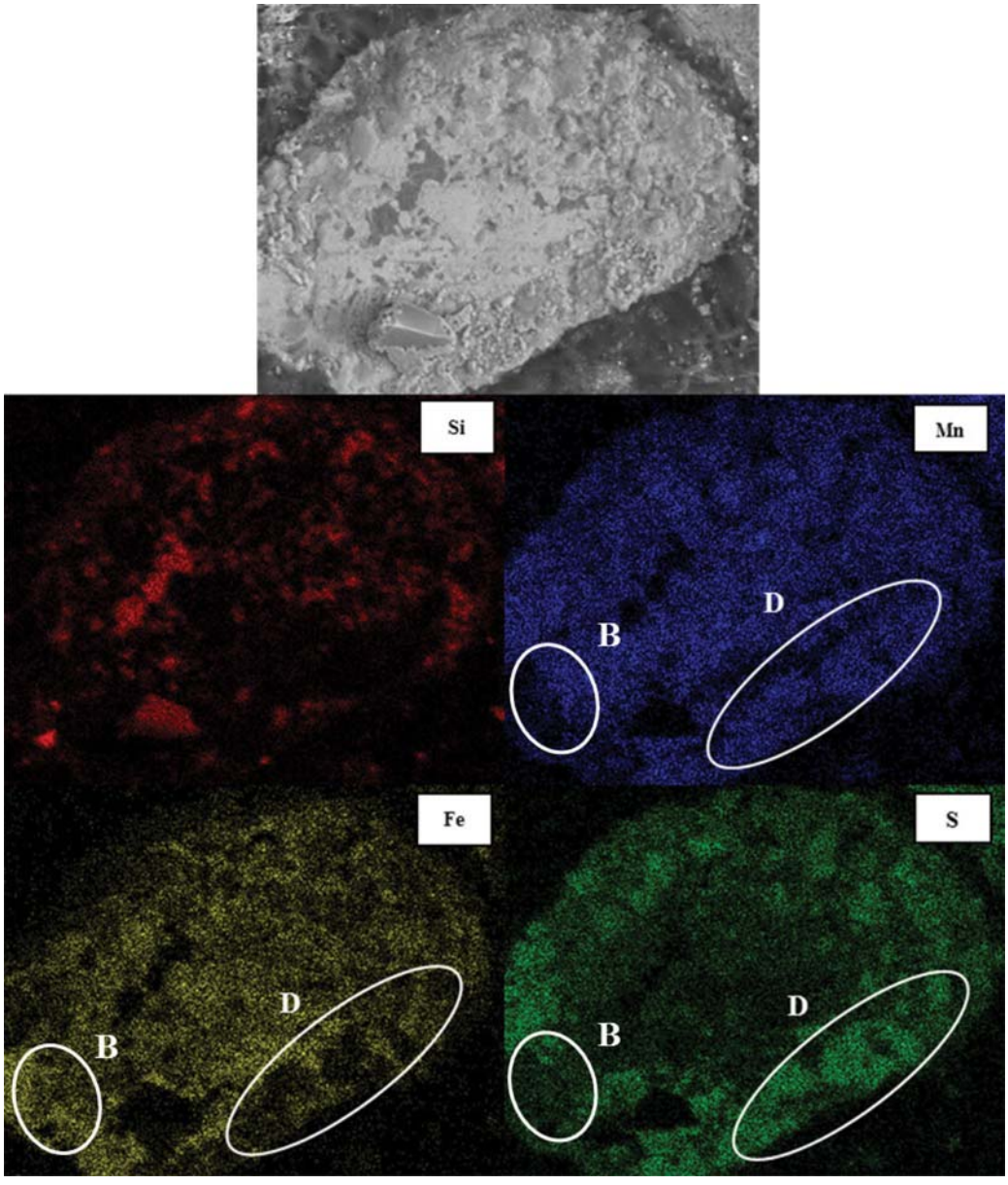

Fig. 7. Backscattered electron images of the sulfated low-grade manganese oxides section and surface scan results of the sulfated low-grade manganese oxides section.

in low-grade manganese oxides (Fig. 7), Si shows a sporadic distribution on the cross-sections, while the Mn, Fe and S are homogeneously distributed on the cross-sections except the Si distribution areas. Differing from the high-grade grade manganese oxide ores, the S elements are not only accumulated on the surface of the particles in the low-grade manganese oxide ores, but also enriched in the particle interior even though the concentration is relatively lower than that on the surface, implying that the flue gas is easier to diffuse into the internal particles. As in previous studies, the SiO_2 has 2D/3D-frame-like structure [30], which reflects that the SiO_2 plays a role of inserting materials to support the internal structure and further strengthen the dispersivity of the MnO_2, which could be given as an explanation of the S distribution in the internal of the particles. The S enriching on the cross-sections surface implies the similar channel blocking effects to the high-grade manganese oxide ores during desulfurization process. Another high content is Fe. It is difficult to distinguish the variations only by a brief view of the distributions of S and Fe elements. Carefully, one can notice that their distributions are quite different in the particles edge, such as B and D areas. It shows that both S and Mn concentrations in D area are consistent and far higher than those of Fe, while those in B area are inverse, demonstrating Fe compounds cannot react with the SO_2 gas, which agrees with the XRD results (Fig. S2) and the previous study [17].

6. N_2 Adsorption Isotherms

Fig. 8(a) and (b) illustrate the nitrogen adsorption isotherms of the both manganese oxide ores before/after desulfurization. All samples show typical type-IV isotherms with H2 hysteresis loops cor-

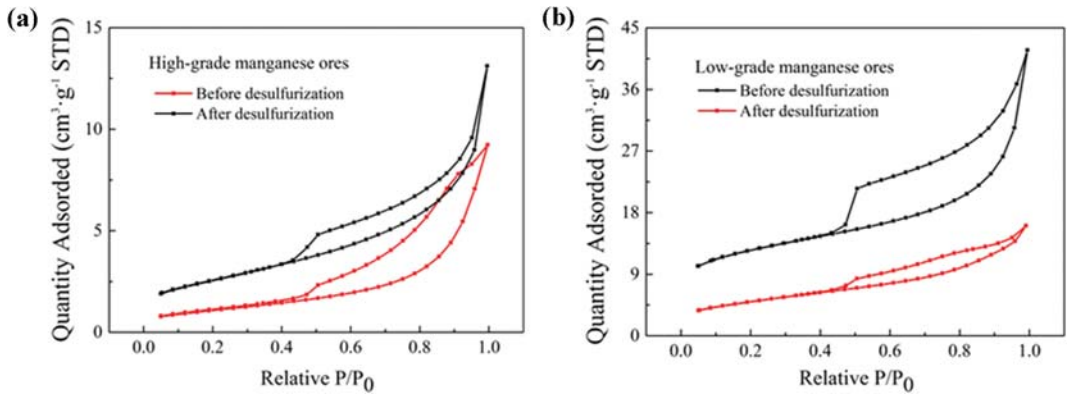

Fig. 8. Nitrogen adsorption/desorption isotherm for (a) high-grade manganese oxide ores and (b) low-grade manganese oxide ores.

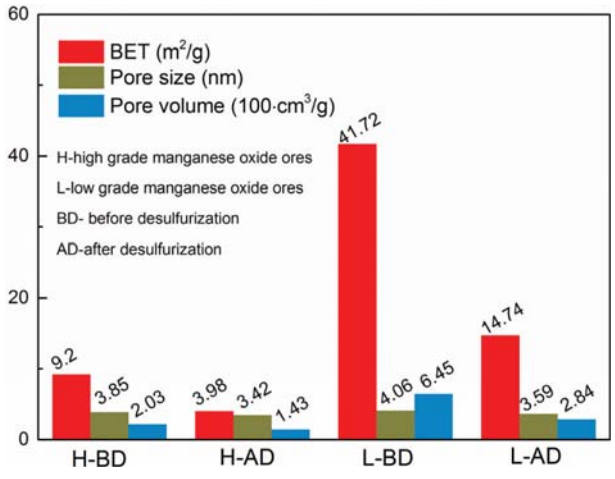

Fig. 9. BET surface area, pore size and pore volume of the manganese oxide ores before/after desulfurization.

responding to a step at relative pressure around P/P_0=0.40-0.60. It is demonstrated that all the samples are mesoporous structure with uniform distribution [31,32]. The BET surface area, average pore size and total pore volume are shown in Fig. 9. The BET surface area for the low-grade manganese oxide ores is 41.72 $m^2 \cdot g^{-1}$, while that for the high-grade manganese oxide ores is only 9.2 $m^2 \cdot g^{-1}$, indicating the significantly larger contact area for the low-grade manganese oxide ores. The high BET surface areas are attributed to the poriferous and lax structure in low-grade manganese oxide ores. As previously reported, a larger surface area could be favorable to the desulfurization reaction [33]. Thus, the low-grade manganese oxide ores show much better desulfurization capability. After desulfurization, the BET surface areas of the both ores decrease to 14.74 and 3.98 $m^2 \cdot g^{-1}$, respectively, which could be related to structural collapse and blocked channel during desulfurization. The average pore size and pore volume also slightly decrease after desulfurization, which further affects the SO_2 diffusion.

CONCLUSIONS

The mechanism of dry flue-gas desulfurization using low and high-grade manganese oxides was comparatively studied. The experimental results revealed that the low-grade manganese oxide ores are porous and exhibit excellent flue gas desulfurization ability. More than 99% of SO_2 removal rate are obtained at the beginning of the reaction for both of the selected high and low grade manganese oxide ores accompanied by $MnSO_4$ produced. However, the SO_2 removal rate sharply drops with prolonging the desulfurization reaction, which is ascribed to the gradual gathering of the generated $MnSO_4$ on the surface or in the pores of the manganese ores. The produced $MnSO_4$ on the surface or in the pores further hinders the diffusion of SO_2. By comparing the SEM/EDS results of the low and high-grade manganese oxides, it is observed that MnO_2 is more dispersed in low-grade ores due to the support of the frame-like structure of the SiO_2. The MnO_2 exposed in the reaction gas leads to the light less or smaller blocking effects of $MnSO_4$. It makes the manganese conversion efficiency and SO_2 removal rate of low-grade ores significantly higher than that of the high-grade ores.

ACKNOWLEDGEMENTS

The authors are very grateful for the financial support from National Natural Science Foundation of China (51574043) and Science and Technology Department of Guangxi Zhuang Autonomous Region (Gangxi special Fund for Scientific Center and Talent Resources, No. 2018AD15002).

SUPPORTING INFORMATION

Additional information as noted in the text. This information is available via the Internet at http://www.springer.com/chemistry/journal/11814.

REFERENCES

1. I. R. Paper, *Korean J. Chem. Eng.*, **28**, 2218 (2011).
2. W. Zhang, X. Li, H. Wang, Y. Song, S. Zhang and C. Li, *Korean J. Chem. Eng.*, **34**, 3132 (2017).
3. J. Hrdlička and T. Dlouhý, *J. Energy Inst.* (2018), DOI:10.1016/j.joei.2018.09.002.

4. R. K. Srivastava and W. Jozewicz, *J. Air Waste Manag. Assoc.*, **51**, 1676 (2001).
5. X. Liu, L. Chen and G. Qi, *Chem. Eng. Technol.*, **41**, 1675 (2018).
6. J. E. Pahlman, S. C. Carlton, R. V. Huff, C. F. Hammel, R. M. Boren and K. P. Kronbeck, US Patent, 6, 974, 565 B2 (2003).
7. J. Bao, L. Yang, W. Sun, J. Geng, J. Yan and X. Shen, *Chem. Eng. Process. Process Intensif.*, **50**, 828 (2011).
8. K. Oikawa, C. Yongsirib, K. Takeda and T. Harimotoa, *Environ. Prog.*, **22**, 67 (2003).
9. Y. Jia, D. Du, X. Zhang, X. Ding and O. Zhong, *Korean J. Chem. Eng.*, **30**, 1735 (2013).
10. Y. Zhao, M. A. Shuang-Chen, X. M. Wang and Z. Qiong, *J. Environ. Sci.*, **15**, 123 (2003).
11. X. Liu, Y. Osaka, H. Huang, J. Li, X. Yang and S. Li, *RSC Adv.*, **6**, 96367 (2016).
12. J. Mo, Z. Wu, C. Cheng, B. Guan and W. Zhao, *J. Environ. Sci. (China)*, **19**, 226 (2007).
13. S. Yao, S. Cheng, J. Li, H. Zhang, J. Jia and X. Sun, *J. Environ. Sci. (China)*, **77**, 32 (2019).
14. S. Kouravand and A. M. Kermani, *J. Clean. Prod.*, **201**, 229 (2018).
15. E. Oh, G. Jung, S. Kim, H. Lee and I. Kim, *Korean J. Chem. Eng.*, **16**, 292 (1999).
16. T. Li, Y. Zhuo, J. Lei and X. Xu, *Korean J. Chem. Eng.*, **24**, 1113 (2007).
17. W. Q. Ye, Y. J. Li, L. Kong, M. M. Ren and Q. Han, *Trans. Nonferrous Met. Soc. China*, **23**, 3089 (2013).
18. J. Zhang, C. You, H. Qi, C. Chen and X. Xu, *Environ. Sci. Technol.*, **40**, 4010 (2006).
19. Z. Pi, B. Shen, J. Zhao and J. Liu, *Ind. Eng. Chem. Res.*, **54**, 10622 (2015).
20. L. Fan, J. Chen, J. Guo, X. Jiang and W. Jiang, *J. Anal. Appl. Pyrolysis*, **104**, 353 (2013).
21. R. Del Valle-Zermeño, J. De Montiano-Redondo, J. Formosa, J. M. Chimenos, M. J. Renedo and J. Fernández, *Energy Fuels*, **29**, 3845 (2015).
22. T. Chen, H. Dou, X. Li, X. Tang, J. Li and J. Hao, *Micropor. Mesopor. Mater.*, **122**, 270 (2009).
23. X. Liu, Y. Osaka, H. Huang, J. Li, Z. He, X. Yang, H. Huhetaoli, S. Li and N. Kobayashi, *RSC Adv.*, **7**, 18500 (2017).
24. S. Bello-Teodoro, R. Pérez-Garibay and J. Bouchard, *Ind. Eng. Chem. Res.*, **53**, 7965 (2014).
25. Y. Osaka, T. Kito, N. Kobayashi, S. Kurahara, H. Huang, H. Yuan and Z. He, *Sep. Purif. Technol.*, **150**, 80 (2015).
26. W. J. W. Bakker, F. Kapteijn and J. A. Moulijn, *Chem. Eng. J.*, **96**, 223 (2003).
27. M. Wu, T. Li, H. Li, H. Fan and J. Mi, *Energy Fuels*, **31**, 13921 (2017).
28. J. Rouquerol, F. Rouquerol, P. Llewellyn, G. Maurin and K. S. Sing, Acad. Press (2013).
29. L. Yang, X. Jiang, Z.-S. Yang and W.-J. Jiang, *Ind. Eng. Chem. Res.*, **54**, 1689 (2015).
30. M. T. Nayakasinghe, N. Sivapragasam and U. Burghaus, *J. Phys. Chem. C*, **122**, 8244 (2018).
31. X. M. Yan, P. Mei, J. Lei, Y. Mi, L. Xiong and L. Guo, *J. Mol. Catal. A Chem.*, **304**, 52 (2009).
32. H. Zhou, G. Li, X. Wang, C. Jin and Y. Chen, *J. Nat. Gas Chem.*, **18**, 365 (2009).
33. Z. Ye, W. Wang, Q. Zhong and I. Bjerle, *Fuel*, **74**, 743 (1995).

Supporting Information

Mechanisms of dry flue-gas desulfurization using natural manganese oxide ores

Yongxiang Chen*, Yunjiao LI*,†, Xinlong Cao*,*, Jianguo Li*, Sanchuan Tang**, Wanqi Ye*, and Xianzhen Zhang***

*School of Metallurgy and Environment, Central South University, Changsha 410083, P. R. China
**Changsha Research Institutes of Mining and Metallurgy, 966 Lushan South Road, Changsha 410012, P. R. China
***Shaanxi Coal Chemical Industry Technology Research Institute Co. Ltd. Xian 710075, P. R. China
(*Received 6 January 2019 • accepted 9 April 2019*)

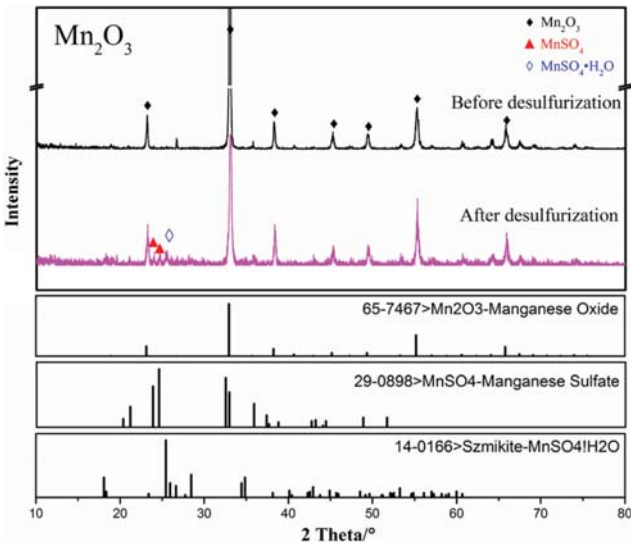

Fig. S1. XRD patterns of the pure Mn_2O_3 before and after desulfurization.

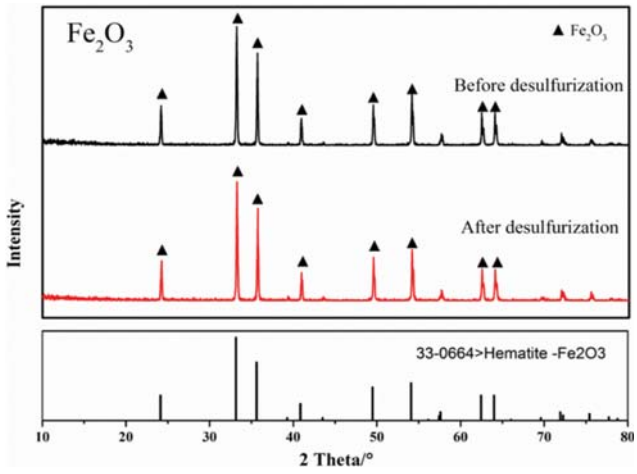

Fig. S2. XRD patterns of the pure Fe_2O_3 before and after desulfurization.